Preparation and Mechanical Characterization of Laser Ablated Single-Walled Carbon-Nanotubes/Polyurethane Nanocomposite Microbeams

Authors:

Louis Laberge Lebel[1,*], Brahim Aissa[2], My Ali El Khakani[2], Daniel Therriault[1]

Author affiliations:

[1]: Center for Applied Research on Polymers and Composites (CREPEC), Mechanical Engineering Department, École Polytechnique of Montréal, C.P. 6079, Succ. Centre-Ville, Montreal (Qc), H3C 3A7, Canada, phone 514-340-4711 x 4419.
[2]: Institut National de la Recherche Scientifique, INRS-Énergie, Matériaux et Télécommunications, 1650 Blvd. Lionel-Boulet, Varennes (Qc), J3X 1S2, Canada, phone: 450-929-8122.

Abstract:

We report on the preparation of nanocomposites consisting of laser synthesized single-walled carbon nanotubes (C-SWNTs) reinforcing a polyurethane. Prior to their incorporation into the polymer matrix, the C-SWNTs were purified, and characterized by means of various techniques. An incorporation procedure in the polymer was developed involving a non-covalent functionalization of the nanotubes by zinc protoporphyrin IX molecule, a covalent functionalization using carboxylic groups graphing and high shear mixing using a three-roll mill. The incorporation of the C-SWNTs into the resin led to an increase of the viscosity and the apparition of a shear thinning behavior. A further adjustment of the shear thinning behavior using fumed silica enabled the direct-write fabrication of microbeams. Mechanical characterization revealed significant increase in both strength (by ~64%) and modulus (by more than 15 times). These mechanical enhancements are believed to be a consequence of both the covalent and the non-covalent functionalizations of the nanotubes.

Keywords:

Nano composites, Carbon nanotubes, Extrusion, Rheology, Mechanical properties

*Corresponding Author:

louis.laberge-lebel@polymtl.ca

INTRODUCTION

Single-walled carbon nanotubes (C-SWNTs) [1,2], with their high aspect ratio, outstanding mechanical [3] and electrical [4] properties, are excellent nanomaterial candidates for polymer nanocomposite reinforcing [5]. For an optimal incorporation of C-SWNTs in polymer matrices, dispersion at the nanoscale level, tailored interaction with the host polymer, and spatial orientation and disposition of this axisymmetric reinforcement are key issues to achieve high-performance nanocomposites. In this context, various dispersion techniques, such as sonication, mechanical shear flow provided by an extruder [6], or a three-roll mixing mill [7], have been investigated. To further disperse the carbon nanotubes into organic matrices, functionalization is often necessary in order to minimize their agglomeration while providing an efficient mechanical link between them and the host polymer matrix. For a polyurethane matrix, covalent functionalization with carboxylic group graphing has been employed [8]. However, extensive modification of the C-SWNT sidewall may destroy the delocalized $\pi-$electron system responsible for their properties [9]. A non-covalent functionalization is possible with polycyclic aromatic hydrocarbons such as pyrene [10], porphyrin [11,12] molecules that adhere to the nanotube sidewall through $\pi-\pi$ interaction [13].

To align the C-SWNT, shear flow combined with the constraining effect of a small-diameter capillary has been used in fiber spinning and stretching [14,15]. This orientation mechanism may also occur during micro-extrusion processes such as the direct-writing [16]. This process consists of the extrusion and robotized deposition of microbeams in a layer-by-layer fashion to form microscopic scaffold structures. During direct-writing,

controlling the rheology is paramount to achieve the desired microbeam shape and periodic patterned structures. Ink with a shear-thinning behavior is preferable due to its ability to flow through the extrusion nozzle at high shear rates as viscosity decreases. After the material is pushed out of the extrusion nozzle, the shear rate it experiences returns to zero, and the deposited microbeam can thus keep its shape depending on the recovered viscosity and elasticity [17]. C-SWNTs can be used to tailor the rheological behavior of polymeric resins. There are indications that when they are added to a polymer, their high aspect ratio causes an increase in viscosity reaching a certain threshold where a rheological percolation network is formed. The latter is responsible for both a viscosity increase and the appearance of a shear-thinning behavior [18,19].

In the present work, C-SWNT reinforced polyurethane nanocomposites were prepared for the direct write fabrication of microbeams followed by the assessment of their mechanical properties. The C-SWNTs were first synthesized by means of the UV-laser ablation method and then covalently and non-covalently functionalized to improve their dispersion within the host polymer matrix. The functionalization was achieved by using zinc protoporphyrin IX molecule (non-covalent) and through carboxylic groups attachment (covalent) to the nanotubes surface during their nitric acid purification process. These groups are expected to interact with the polar groups on the polyurethane backbone [8]. The mixing procedure presented herein resulted in a viscosity behavior suitable for the direct-write fabrication of microbeams. Their mechanical properties were systematically tested, through their subjection to tensile loading. We were thus able to point out the beneficial effect of an enhanced interaction between the polymer and reinforcing nanotubes through

additional covalent functionalization on the mechanical properties of the nanocomposite microbeams.

EXPERIMENTAL

C-SWNT Synthesis, purification and characterizations

The C-SWNTs were synthesized from the UV-laser (KrF excimer) ablation of a graphite target appropriately doped with Co/Ni metal catalyst. The synthesis was performed under a controlled argon atmosphere at a furnace temperature of 1100°C (more details on the C-SWNTs were reported elsewhere [20]). A reflux of five hours in a 3 molar HNO_3 (Sigma Aldrich) solution was used to purify the as-grown (AG) material. The purified (PU) C-SWNTs were then rinsed and filtered using a 0.22 μm porous poly-tetrafluoroethylene membrane (Filter type-GV, Millipore corp). The C-SWNTs were characterized by a variety of techniques, including bright field transmission electron microscopy (TEM by means of a Jeol JEM-2100F FEG-TEM 200 kV-microscope); Raman spectroscopy (microRaman, Renishaw Imaging Microscope Wire), in the backscattering geometry, using the 514.5 nm wavelength of an Ar^+ laser as an excitation line; X-ray photoelectron spectroscopy (XPS, Escalab 220i-XL system, VG instruments) using the monochromatic Al Kα radiation as the excitation source (1486.6 eV, full width at half-maximum of the Ag 3d5/2 line = 1eV at 20 eV pass energy); and thermogravimetry analysis (TGA 2950, TA Instruments) under air flow with a heat ramp of 15°C/min 900°C.

Nanocomposite preparation

The nanocomposite material is a mixture of the synthesized C-SWNTs with a commercially available UV-curable polyurethane matrix (NEA123MB, Norland Products).

zinc protoporphyrin IX (ZnPP, Sigma-Aldrich) was used to facilitate the dispersion of the C-SWNTs. A specific amount of C-SWNT was sonicated (Ultrasonic cleaner 8891, Cole-Parmer) in a solution of 0.1 mM of ZnPP in dichloromethane (DCM, Sigma-Aldrich) for 30 minutes. Polyurethane was then slowly added to the C-SWNT solution while mixing at 800 RPM for 30 min over a stirring hot plate (Model SP131825, Barnstead international). After complete solvent evaporation, the nanocomposite mixture was passed several times in a three-roll mixer mill (80E, Exakt) where the gap between the rolls and the speed of the apron roll were controlled [21]. The total procedure consisted of 5 passes at a gap of 25 μm and speed 200 rpm, 5 passes at a gap of 15 μm and speed 200 rpm, and 9 passes at a gap of 5 μm and speed 250 rpm. Fumed silica nanoparticles were also added to augment the viscosity and to yield a shear-thinning behavior [22].The nanocomposite was slowly added to a fumed silica nanoparticle (Aerosil 200, Degussa) solution in DCM while mixing over a stirring hot plate. Finally, the mixture was poured in syringe barrels (3cc, EFD) where the DCM solvent was fully evaporated. The whole procedure produced UV-Curable nanocomposites containing 0.5 wt% of C-SWNTs (either AG or PU) and 5 wt% of Fumed silica. The microscopic scale dispersion was characterized by observing a ~10 μm thick film under transmission light optical microscope using the 40X objective (BX-61, Olympus) and image analysis software (Image-Pro Plus, Media Cybernetics Inc).

Viscosity characterization

An experimental method based on capillary viscosimetry was developed to measure the process-related apparent viscosity of the pure polyurethane, the polyurethane containing 5 wt% of fumed silica, and the nanocomposites at different stages of the mixing procedure.

To obtain different strain rate and shear stress combinations, five continuous lines (length of 384 mm) of material were extruded through a micronozzle (5127-0.25-B, Precision Stainless Steel Tips, EFD) at 5 different pressures over glass substrates, with calibrated displacement speeds. Material depositions were done using a computer controlled robot (I&J220-4, I&J Fisnar) moving a dispensing apparatus (HP-7X, EFD) along the *x*, *y* and *z* principal axis. After deposition, the material was cured through its exposure to UV radiation emitted by two UV light emitting diodes (LED, wavelength of 365 nm, 70 mW/cm^2, NCSU033A, Nichia). The flow rate of the extrusion process was calculated by multiplying the displacement speed of the deposition apparatus to the cross section of the deposited filaments, characterized using a high resolution optical sensor (CHR 150, Stil). The wall shear rate, apparent wall shear stress and process apparent viscosity were calculated using a method inspired from the work of Bruneaux and co-workers [23].

Mechanical Characterization

The UV-assisted direct write method was used to fabricate mechanical coupons from the polyurethane, the AG and PU nanocomposites in order to assess the mechanical reinforcement of polyurethane by C-SWNTs. For all three materials, the viscosity enhanced formulations (i.e., containing fumed silica) were used due to their shear-thinning behavior, which is a prerequisite to the efficient direct-write manufacturing method. Three microbeams were suspended over the three mm gap between two rectangular pads of the same material. The microbeams were cured using UV exposure while being extruded over the gap by a robot that moved the extrusion apparatus in a linear direction. The deposited microbeams were tested in a dynamic mechanical analyzer (DMA, DMA2980, TA

instruments) using a film tension clamp. The two pads were used to fix the microbeam. The two outer microbeams, deposited mainly to facilitate the manipulation of the whole coupon, were cut after the coupon installation in the DMA. After applying a pre-charge of five mN, the microbeams were tested in tension with a constant loading rate set to reach failure within ~ 20 seconds. Values of the breaking strength and initial modulus were calculated from the force/displacement response and the cross-section measurements of the failure plane. The microbeam cross-section dimensions were measured through digital image analysis of optical microscope images (BX-61, Olympus and using the software Image-Pro plus V5, Media Cybernetics).

RESULTS AND DISCUSSION

Carbon nanotube characterizations

Fig. 1a shows a TEM micrographs of the AG nanotubes deposit, where bundles of C-SWNTs are clearly seen to consist of few single-walled nanotubes (the diameter of the single tubes is ~1.2 nm). In conjunction with the C-SWNTs, other carbon nanostructures (e.g., nanocages, nanonions, and nanohorns) can be also produced by the laser process, as previously reported [20]. Moreover, metal catalyst nanoparticles are also expected to be present in the AG C-SWNTs deposits. The darker spots of Fig. 1a represent either dense C nanostructures or CoNi metal catalyst particles wrapped within C nanostructures. The nanotubes purification permit to eliminate a large part of the catalyst residues and other C nanostructures with a high density of structural defects, as illustrated in Fig. 1b. The PU C-SWNTs are found to consist of bundles having diameters in the 2-10 nm range and lengths in the order of few μms leading thereby to aspect ratios of at least 3 orders of magnitudes.

Fig. 2a shows typical Raman spectra of AG and PU C-SWNTs samples, where scattering peaks appearing in the low (100-300 cm^{-1}) and high (~1600 cm^{-1}) frequency regions constitute the typical signature of the presence of SWNTs. These absorption bands correspond to the radial breathing mode (RBM) and the tangential vibrating mode (G), respectively. The RBM peak centered at 182 cm^{-1} is attributed to the strong presence of C-SWNTs having a mean diameter of 1.2 nm [24], in accordance with the measurements from direct TEM observations. The D peak centered around 1350 cm^{-1} is due to the presence of amorphous or disordered carbon structures. The rather high G-to-D peak intensity ratio for the AG samples indicates the overall good-quality of the C-SWNTs. Nevertheless, it is worth noting that this ratio is seen to increase after subjecting the nanotubes to the purification process (i.e., PU samples). This suggests that the nitric acid oxidization treatment created structural defects in the nanotubes. This interpretation is supported by the XPS data, which show that the C1s core level peak consists of three clear components, while that of AG-SWNTs samples exhibit a relatively narrow C=C peak (Fig. 2b). For the PU nanotubes, in addition to the main component centered around 284.5 eV, which is due to the sp^2 C=C bonding forming the bulk structure of C-SWNTs, the two shoulders appearing at 286 eV and 288 eV were attributed to C-O and/or C-NHx bonds and to COO group of carboxylic acid groups [25,26]. The XPS results confirm that the purification process has led to carboxylic groups grafting onto the C-SWNTs surfaces (i.e., covalent functionalization).

Finally, our carbon nanotubes were also analyzed by means of thermogravimetry. Fig. 3 shows TGA curves and their associated differentiated curves (DTGA) of both AG

and PU C-SWNTs. For the AG material, some weight loss (only few % of the analyzed mass) starts at ~450°C while the main part of the deposit oxidizes in the 650-850°C range. For the PU nanotubes, the first oxidation starts at lower temperatures (~370°C) and represents almost 40% of the deposit, and the second oxidation occurs in the 650-850°C (as for the AG nanotubes but to a lesser extent). These results show that an important part of the PU nanotubes becomes more defective due to the acid nitric oxidation and hence more vulnerable to oxidation. For both the AG and PU materials, the second oxidation occurring in the 650-850°C temperature range is believed to be due to non-defective nanotubes and other graphitized carbon nanostructures (Fig. 1). This temperature range corresponds to those reported elsewhere for the burning temperature of C-SWNT (of which ignition occurs ~600°C [27]) and the oxidation of highly-graphitized carbon fibers (~800°C [28]). Moreover, our UV-laser synthesized C-SWNTs have been shown to exhibit a rather high oxidation resistance as some of them survived annealing temperatures in excess of 800°C [29]. The oxidation of an important part of the purified C-SWNTs at relatively low temperatures (~ 370°C) is a consequence of the presence of a higher density of defects produced by the nitric acid purification process, in accordance with the above-discussed XPS and Raman results.

Nanocomposite preparation

The AG and PU C-SWNTs were dispersed inside a UV-curable polyurethane resin according to the method described in the experimental section. Fig. 4 shows optical microscope images of the obtained SWNTs/polymer nanocomposite films, in which dark spots are observed. These spots (of which average size was estimated to ~1.3 μm for both

AG and PU samples) are believed to be aggregates of carbonaceous materials or C-SWNTs entangled around larger carbon particles. Nevertheless, the largest spots observed diminished in size from ~12 to ~7 .2 μm average diameter when the nanotubes are purified compared to AG samples (for the same 0.5 wt% C-SWNTs content in the polyurethane matrix). From Fig. 4 and through the distribution of the visible dark spots, one can assume that the C-SWNTs, along with their associated agglomerates, were uniformly dispersed in the polyurethane matrix. Nevertheless, it is difficult to ascertain that all the C-SWNTs are exfoliated and dispersed at the nanoscale level.

Viscosity characterization

Viscosity characterization was performed on the AG and PU nanocomposite materials at different stages during the mixing procedure since the apparent viscosity is a good indicator of the dispersion of the nanotubes. In addition, the direct-write assembly of nanocomposite materials requires viscous and shear-thinning behaviors. The viscosity measurements of the polymer and the nanocomposite at different blending steps are presented in Fig. 5. The indication 0 wt% stands for pure polyurethane, 0.5 wt%AG for the AG-C-SWNT/polyurethane blend (Fig. 5a) and the 0.5 wt%PU for PU-C-SWNT/polyurethane blend (Fig. 5b). The suffix 3R represents the three-roll mixing whereas FS indicates the addition of fumed silica stages. The process related apparent viscosity (η_{app}) values were plotted on a log-log graph as a function of the shear rate ($\dot{\gamma}$) and fitted with a power law fluid relationship according to the following equation:

$$\eta_{app} = m\left(\dot{\gamma}\right)^{(1-n)} \tag{1}$$

Table 1 lists the calculated values of the power-law indexes n as an indication of the viscosity behavior with respect to the strain rate. The samples 0 wt%, 0.5 wt%AG and 0.5 wt%AG-3R have an index near 1 showing a Newtonian behavior as the value of viscosity does not vary over the strain rates investigated. All the other measured samples have a calculated value of $n < 1$ due to their shear thinning behavior.

The first mixing stage consisted of the incorporation of the AG and PU nanotubes in the polyurethane resin. After the nanotube incorporation (0.5 wt%AG and 0.5 wt%PU), the measured viscosity did not significantly increase compared to the unloaded polyurethane (0 wt%), and the rheological behavior of the AG-SWNTs/resin nanocomposite was still Newtonian. This was due to micro-sized aggregations of C-SWNT and impurities that could not form a viscosity percolated network. A slight shear-thinning behavior was observed for the PU-SWNTs/resin nanocomposite (0.5 wt%PU, $n = \sim 0.85$). This can be explained by the higher quantity of nanotubes that forms a viscosity percolated network.

After the three-roll mixing, a dramatic viscosity increase was observed for both the AG and PU C-SWNT blends, indicating that the three-roll mill reduced the size of aggregates and successfully dispersed the added material. However, the calculated viscosity indexes after this mixing stage remained unchanged. In fact, it has been observed that the shear-thinning behavior of a nanocomposite, caused by a rheological percolation network, occurs when the critical percolation concentration is reached [18]. The latter is, in turn, more sensitive to the aspect ratio (i.e.; length over diameter) of the reinforcing nanomaterial rather than to its actual size [30]. Thus, it can be argued that the three-roll mixing step did not generate more high-aspect-ratio entities (i.e., individual nanotubes).

The incorporation of fumed silica particles further increased the viscosity and changed the rheological behavior, as indicated by the viscosity index n which was found to be of ~0.5. The same response is observed at different intensities for the three blends 0.5 wt%AG-3R-FS, 0.5 wt%PU-3R-FS and the 0 wt%-FS whose power-law index values are comparable. This effect is the result of a network formation of hydrogen bonded fumed silica particles that impart a gel-like rheological behavior to the mixture at rest. The apparent viscosity diminishes under application of a moderate shear force destroying the weakly bounded network [31]. The resulting shear-thinning behavior is a prerequisite for the successful manufacturing of the microbeams coupons used in the present work. This rheological property permitted the extrusion of the nanocomposite through a micronozzle, and, due to the reduction of the shear rate after extrusion, the viscosity increase allowed the curing of the microbeam with a defined shape through UV radiation exposure.

Nanocomposite Microbeams Tensile Response

The polyurethane, AG and PU mixtures containing fumed silica particles were successfully deposited between two tabs for the fabrication of cylindrical microbeams (diameter $d \approx 150\,\mu\text{m}$ and length $l \approx 3\,\text{mm}$). Fig. 6 presents various aspects related to the mechanical characterization under DMA tensile tests comprising a typical image of the original microbeam coupons used in this study (Fig. 6a), a representative set of stress-strain curves (Fig. 6b), the calculated modulus and failure strength (Fig. 6c), and a cross-sectional image of the microbeam failure (Fig. 6d). The stress strain curves (Fig. 6b) indicate a clear change in the mechanical behavior between the unloaded polyurethane microbeams and the nanocomposite ones. The unloaded material (0 wt%-FS) exhibits a non-linear response of

the stress under strain and experiences an elongation as long as 120% ± 20% before rupture. In contrast, the nanocomposite response becomes elastic and linear until breakage, which is reached at rather shorter elongations of 12% ± 4% for the 0.5 wt%AG-3R-FS and 7.2% ± 0.6% for the 0.5 wt%PU-3R-FS. This radically different behavior in comparison with the unloaded polyurethane is attributed to the C-SWNT incorporation and a significant stress transfer between the host matrix and the nano-reinforcement.

The improved mechanical interaction is indicated by the value of the initial modulus (Fig. 6c) that is shown to increase by 10 times for the AG C-SWNT and more than 15-fold for the PU C-SWNT nanocomposite compared with the initial modulus of the 0 wt%-FS polyurethane. These increases are in accordance with the beneficial effect on the elastic modulus observed when loading polymers with C-SWNTs [5]. Moreover, the failure strength of both AG and PU C-SWNTs nanocomposites (~40 MPa) also increased by ~ 64% in comparison with the value of the 0 wt%-FS. The average strength of the nanocomposite was the same for AG and PU C-SWNT nanocomposite materials since the same rupture mechanism was observed in all the nanocomposite microbeams. The rupture is most probably triggered by the presence of aggregates that act as stress concentrators. This is illustrated in Fig. 6d, where a typical fracture surface is seen with three clearly discernable regions, namely, a crack initiator represented by a dark spot (upper right corner of the section), a region of slow crack propagation around this dark spot, and a region of dramatic crack propagation for the rest of the fracture surface.

In an attempt to understand the possible interaction mechanisms governing the interaction of the C-SWNTs and the polyurethane matrix, the results presented in this study

can be interpreted in the light of the mechanisms proposed by Sahoo et al. [8]. As summarized in Fig. 7, the interaction between the polyurethane backbone and reinforcing nanotubes is highly likely due to both non-covalent and covalent functionalizations of the C-SWNTs. For the AG-SWNTs, the interaction mechanism relies on the use of the ZnPP molecules that are composed of a series of flat cycles of carbon which, in turn, can interact with the nanotube walls through $\pi - \pi$ interactions. The other end of the molecules has two carboxylic groups, which are capable of interacting with the polyurethane –CONH- groups on the polymer backbone. The formation of such chemical bonding through the use of the ZnPP non-covalent functionalization is believed to be at the origin of the significant rigidity increase exhibited by the nanocomposite microbeams compared to the unloaded polyurethane ones. For the PU-SWNTs, the purification induced covalent grafting of carboxylic groups at the surface of the nanotubes, as revealed by XPS analyses, offers additional interaction possibility with the polymer matrix. Hence, the higher increase in the initial modulus for the PU C-SWNT material compared to that of the AG material is attributed to two factors: (i) the purification procedure improved the C-SWNT concentration in the soot; and (ii) the carboxylic group grafting increased SWNTs anchoring to the polymer, leading thereby to an enhanced stress transfer between the polymer and the nanotubes. Another contribution may come from the beneficial orientation of the C-SWNTs that could occur during the extrusion of the nanocomposite through the micro-nozzle. However, other characterizations, such as polarized Raman spectroscopy [32], should be performed to quantify the orientation of the C-SWNT reinforcement with respect to the microbeam axis.

CONCLUSIONS

Nanocomposites were prepared for the successful fabrication of suspended microbeams made of polyurethane reinforced by either AG- or PU-laser-synthesized C-SWNTs. Challenging issues such as nanotubes functionalization and dispersion, controlled mixing of the nanotubes with the polyurethane matrix, optimizing the viscosity of the resulting nanocomposite, were dealt with. In particular, we pointed out that the concomitant covalent and non-covalent functionalizations of the nanotubes are at the origin of an enhanced stress transfer between the polymer and the nanotubes. The mechanical testing of the fabricated microbeams demonstrated the improvement (by more than 15 times) of the modulus of the PU-C-SWNT/polymer nanocomposite compared to the unloaded polyurethane resin. The failure strength was found to be limited probably by the presence of aggregates in the microbeams. The presence of such aggregates would also limit reaching the shear thinning behavior state of the nanocomposite because of the difficulty to form a viscosity percolated network. Using an ultracentrifugation step after the non-covalent functionalization would help remove the aggregates, and potentially lead to a strong shear-thinning behavior without the assistance of fumed silica particles. Finally, even if the nanocomposite ingredients and their optimized mixing need to be further improved, the material preparation demonstrated here opens new prospects for the direct-write microfabrication of C-SWNT based nanocomposites for the achievement of tailored microstructures for micromechanical applications.

ACKNOWLEGEMENTS

The authors acknowledge the financial support from FQRNT (Le Fonds Québécois de la Recherche sur la Nature et les Technologies) and NSERC (the Natural Sciences and Engineering Research Council of Canada). They also acknowledge the support of Profs. Nakai and Hamada (from Kyoto Institute of Technology) for some of the mechanical testing performed in their laboratory.

REFERENCES

1. Bethune DS, Kiang CH, de Vries MS, Gorman G, Savoy R, Vazquez J, Beyers R. Cobalt-catalysed growth of carbon nanotubes with single-atomic-layer walls. Nature 1993;**363**(6430):605.
2. Iijima S, Ichihashi T. Single-shell carbon nanotubes of 1-nm diameter. Nature 1993;**364**(6439):737.
3. Qian D, Wagner GJ, Liu WK, Yu M-F, Ruoff RS. Mechanics of carbon nanotubes. Applied Mechanics Reviews 2002;**55**(6):495-532.
4. Tans SJ, Devoret MH, Dai H, Thess A, Smalley RE, Georliga LJ, Dekker C. Individual single-wall carbon nanotubes as quantum wires. Nature 1997;**386**(6624):474-7.
5. Coleman JN, Khan U, Blau WJ, Gun'ko YK. Small but strong: A review of the mechanical properties of carbon nanotube-polymer composites. Carbon 2006;**44**(9):1624-1652.
6. Thostenson ET, Chou T-W. Aligned multi-walled carbon nanotube-reinforced composites: Processing and mechanical characterization. Journal of Physics D: Applied Physics 2002;**35**(16):77-80.
7. Gojny FH, Wichmann MHG, Kopke U, Fiedler B, Schulte K. Carbon nanotube-reinforced epoxy-composites: Enhanced stiffness and fracture toughness at low nanotube content. Composites Science and Technology 2004;**64**(15 SPEC ISS):2363-2371.
8. Sahoo NG, Jung YC, Yoo HJ, Cho JW. Effect of functionalized carbon nanotubes on molecular interaction and properties of polyurethane composites. Macromolecular Chemistry and Physics 2006;**207**(19):1773-1780.
9. Frankland SJV, Caglar A, Brenner DW, Griebel M. Molecular simulation of the influence of chemical cross-links on the shear strength of carbon nanotube-polymer interfaces. Journal of Physical Chemistry B 2002;**106**(12):3046-3048.
10. Chen RJ, Zhang Y, Wang D, Dai H. Noncovalent sidewall functionalization of single-walled carbon nanotubes for protein immobilization. Journal of the American Chemical Society 2001;**123**(16):3838-3839.
11. Satake A, Miyajima Y, Kobuke Y. Porphyrin-carbon nanotube composites formed by noncovalent polymer wrapping. Chemistry of Materials 2005;**17**(4):716-724.

12. Li H, Zhou B, Lin Y, Gu L, Wang W, Fernando KAS, Kumar S, Allard LF, Sun Y-P. Selective Interactions of Porphyrins with Semiconducting Single-Walled Carbon Nanotubes. Journal of the American Chemical Society 2004;**126**(4):1014-1015.
13. Murakami H, Nakashima N. Soluble carbon nanotubes and their applications. Journal of Nanoscience and Nanotechnology 2006;**6**(1):16-27.
14. Sandler JKW, et al. A comparative study of melt spun polyamide-12 fibres reinforced with carbon nanotubes and nanofibres. Polymer 2004;**45**(6):2001-2015.
15. Haggenmueller R, Gommans HH, Rinzler AG, Fischer JE, Winey KI. Aligned Single-Wall Carbon Nanotubes in Composites by Melt Processing Methods. Chemical Physics Letters 2000;**330**(3-4):219-225.
16. Lewis JA, Gratson GM. Direct writing in three dimensions. Materials Today 2004;**7**(7):32-39.
17. Therriault D, Shepherd RF, White SR, Lewis JA. Fugitive inks for direct-write assembly of three-dimensional microvascular networks. Advanced Materials 2005;**17**(4):395-399.
18. Du F, Scogna RC, Zhou W, Brand S, Fischer JE, Winey KI. Nanotube networks in polymer nanocomposites: Rheology and electrical conductivity. Macromolecules 2004;**37**(24):9048-9055.
19. Potschke P, Fornes TD, Paul DR. Rheological behavior of multiwalled carbon nanotube/polycarbonate composites. Polymer 2002;**43**(11):3247-3255.
20. Braidy N, El Khakani MA, Botton GA. Carbon nanotubular structures synthesis by means of ultraviolet laser ablation. Journal of Materials Research 2002;**17**(9):2189-2192.
21. Thostenson ET, Chou T-W. Processing-structure-multi-functional property relationship in carbon nanotube/epoxy composites. Carbon 2006;**44**(14):3022-9.
22. *Industrial brochure of Aerosil in adhesives and sealants*, 2004: Frankfurt, Germany
23. Bruneaux J, Therriault D, Heuzey MC. Micro-extrusion of organic inks for direct-write assembly. Journal of Micromechanics and Microengineering 2008;**18**(11):115020 (11 pp.).
24. Bandow S, Asaka S, Saito Y, Rao AM, Grigorian L, Richter E, Eklund PC. Effect of the growth temperature on the diameter distribution and chirality of single-wall carbon nanotubes. Physical Review Letters 1998;**80**(17):3779-82.
25. Baker SE, Cai W, Lasseter TL, Weidkamp KP, Hamers RJ. Covalently Bonded Adducts of Deoxyribonucleic Acid (DNA) Oligonucleotides with Single-Wall Carbon Nanotubes: Synthesis and Hybridization. Nano Lett. 2002;**2**(12):1413-1417.
26. Okpalugo TIT, Papakonstantinou P, Murphy H, McLaughlin J, Brown NMD. High resolution XPS characterization of chemical functionalised MWCNTs and SWCNTs. Carbon 2005;**43**(1):153-61.
27. Rinzler AG, et al. Large-scale purification of single-wall carbon nanotubes: Process, product, and characterization. Applied Physics A: Materials Science & Processing 1998;**67**(1):29-37.
28. Dresselhaus MS, Dresselhaus G, Sugihara K, Spain IL, Goldberg HA, *Graphite Fibers and Filaments*. 1998, Berlin: Springer-Verlag.
29. Yi JH, Aissa B, El Khakani MA. Ultra-high oxidation resistance of suspended single-wall carbon nanotube bundles grown by an "all-laser" process. Journal of Nanoscience and Nanotechnology 2007;**7**(10):3394-3399.

30. Balberg I, Binenbaum N, Wagner N. Percolation thresholds in the three-dimensional sticks system. Physical Review Letters 1984;**52**(17):1465-8.
31. Raghavan SR, Walls HJ, Khan SA. Rheology of silica dispersions in organic liquids: New evidence for solvation forces dictated by hydrogen bonding. Langmuir 2000;**16**(21):7920-7930.
32. Gommans HH, Alldredge JW, Tashiro H, Park J, Magnuson J, Rinzler AG. Fibers of aligned single-walled carbon nanotubes: Polarized Raman spectroscopy. Journal of Applied Physics 2000;**88**(5):2509-14.

FIGURES

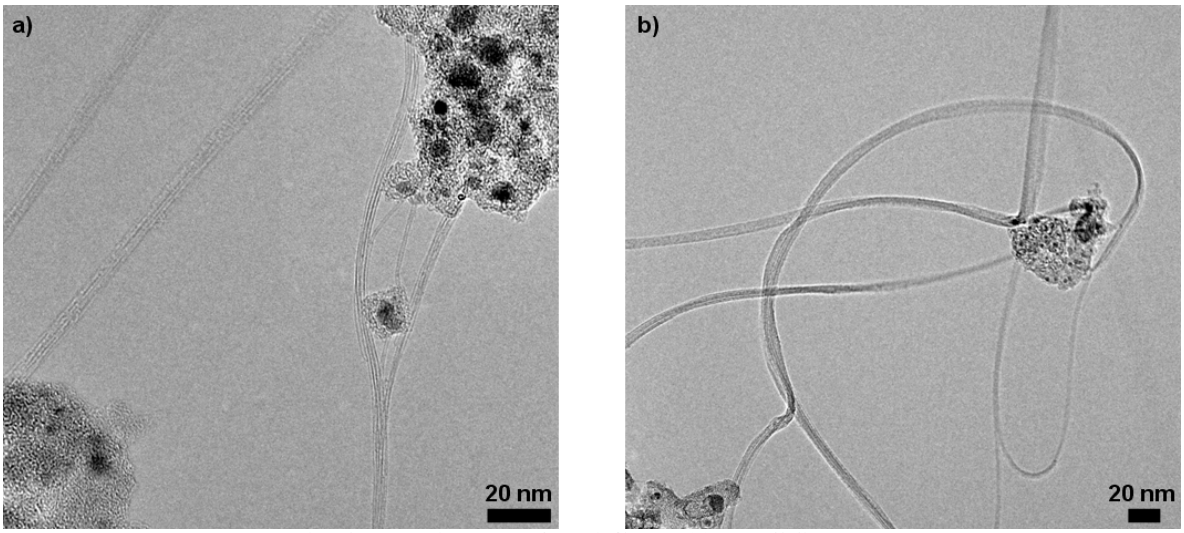

Fig. 1. TEM images of (a) AG and (b) PU C-SWNTs.

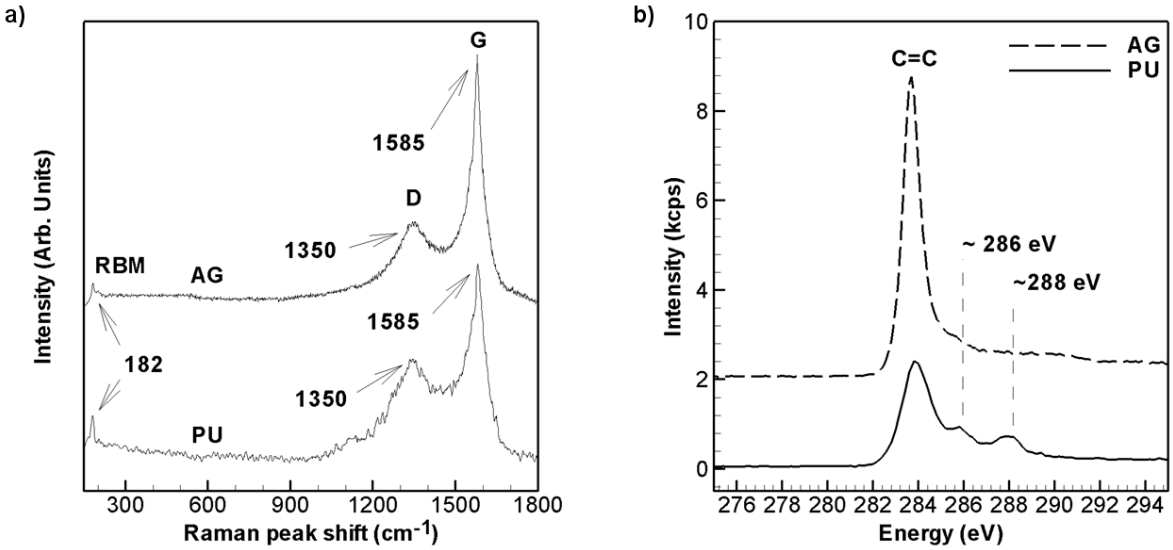

Fig. 2. (a) Raman spectra and (b) Photoelectron spectra of C1s of AG and PU C-SWNTs.

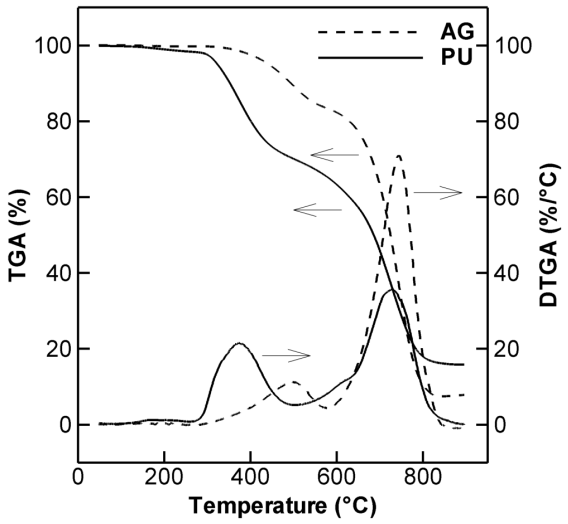

Fig. 3. Thermogravimetric analysis of AG and PU C-SWNT materials.

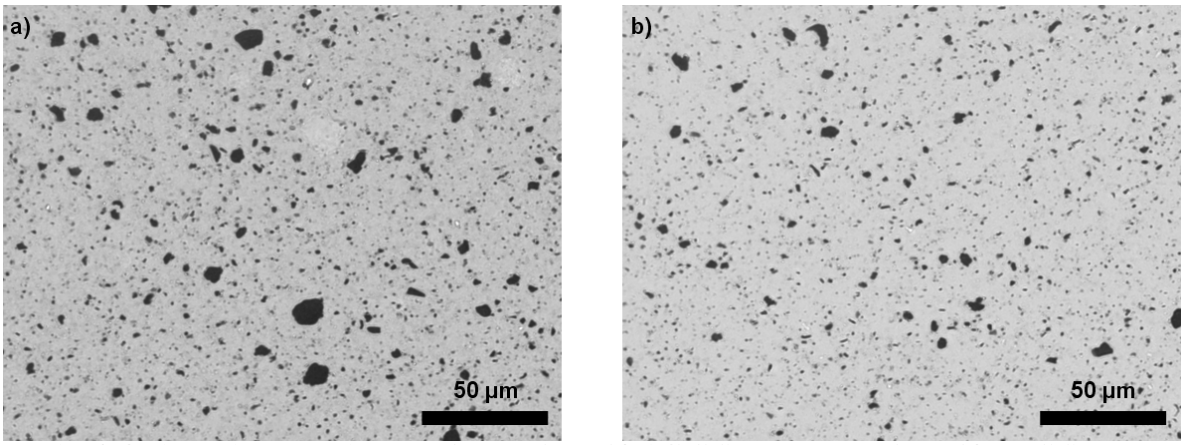

Fig. 4. Optical microscope images of the (a) 0.5 wt% AG C-SWNT and (b) 0.5 wt% PU C-SWNT nanocomposite blends after the complete mixing procedure.

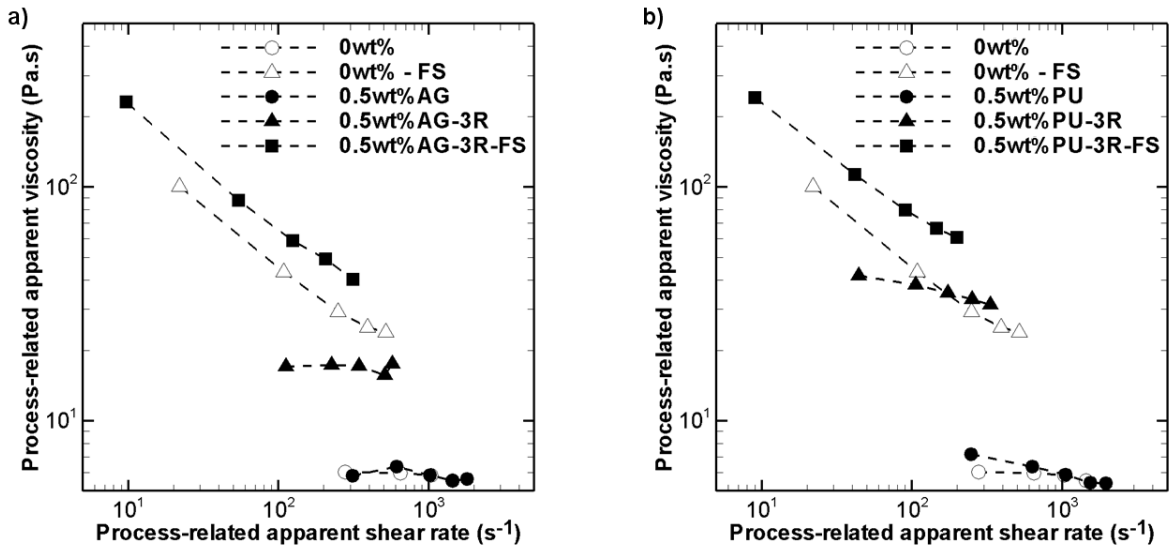

Fig. 5. Viscosity characterizations of (a) AG and (b) PU nanocomposite blends.

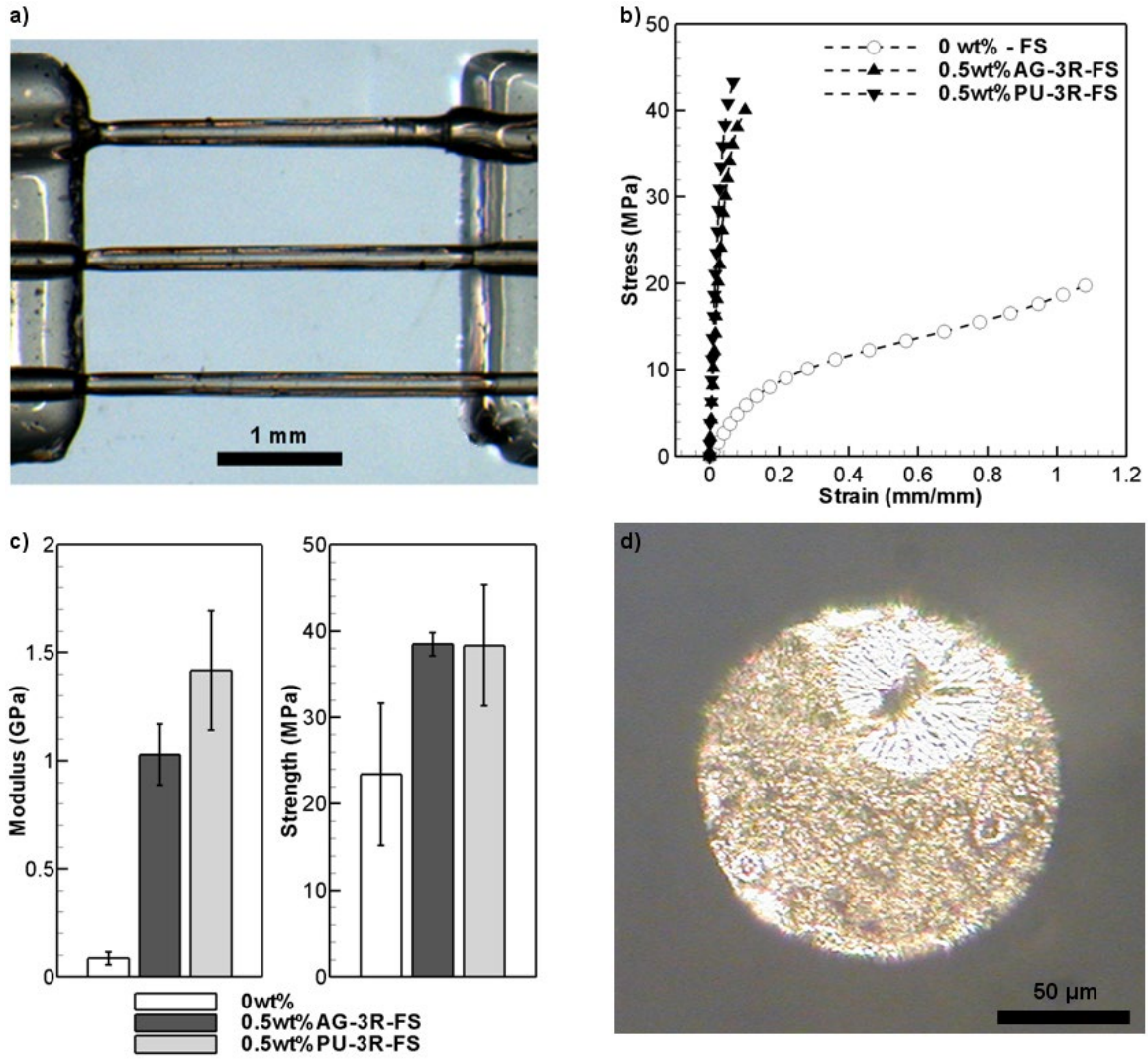

Fig. 6. Mechanical characterization of the nanocomposite blends: (a) mechanical coupon comprising three suspended microbeams over a three mm gap between the fixing tabs, (b) Typical stress-strain curves, (c) Bar graphs showing the values of initial modulus and ultimate stress, (d) Fracture plane of a 0.5 wt% PU nanocomposite microbeam.

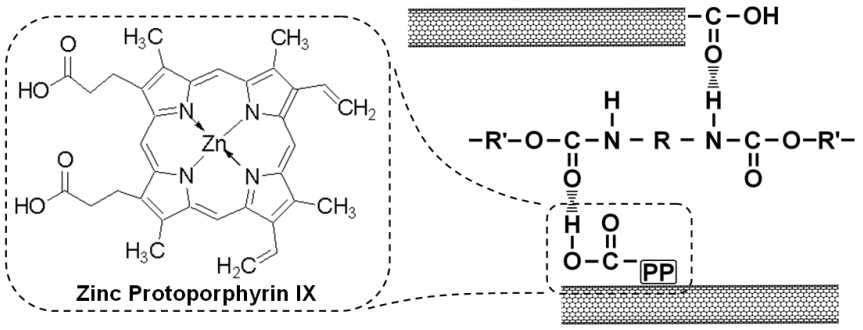

Fig. 7. Schematic of two proposed interaction mechanisms between polyurethane and C-SWNT using grafted carboxylic group (covalently bonded) on the C-SWNT wall [8] or through the non-covalently attached zinc protoporphyrin IX molecule to the C-SWNT wall.

TABLES

Table 1. Viscosity indexes of nanocomposite blends.

Sample	Viscosity index n
0 wt%	0.95
0 wt% – FS	0.53
0.5 wt%AG	0.96
0.5 wt%AG – 3R	0.98
0.5 wt%AG – 3R – FS	0.50
0.5 wt%PU	0.85
0.5 wt%PU – 3R	0.86
0.5 wt%PU – 3R – FS	0.55